ACS Chemical Neuroscience

Research Article

pubs.acs.org/chemneuro

Comparative Modeling of the Human Monoamine Transporters: Similarities in Substrate Binding

Heidi Koldsø,[†,§] Anja B. Christiansen,[‡] Steffen Sinning,[‡] and Birgit Schiøtt*[,†]

[†]Center for Insoluble Protein Structures (*in*SPIN) and Interdisciplinary Nanoscience Center (*i*NANO), Department of Chemistry, Aarhus University, Langelandsgade 140, 8000 Aarhus C, Denmark

[‡]Laboratory of Molecular Neurobiology, Centre for Psychiatric Research, Aarhus University Hospital, Skovagervej 2, 8240 Risskov, Denmark

Supporting Information

ABSTRACT: The amino acid compositions of the substrate binding pockets of the three human monoamine transporters are compared as is the orientation of the endogenous substrates, serotonin, dopamine, and norepinephrine, bound in these. Through a combination of homology modeling, induced fit dockings, molecular dynamics simulations, and uptake experiments in mutant transporters, we propose a common binding mode for the three substrates. The longitudinal axis of the substrates is similarly oriented with these, forming an ionic interaction between the ammonium group and a highly conserved aspartate, Asp98 (serotonin transporter, hSERT), Asp79 (dopamine transporter, hDAT), and Asp75 (norepinephrine transporter, hNET). The 6-position of serotonin and the *para*-hydroxyl groups of dopamine and norepinephrine were found to face Ala173 in hSERT, Gly153 in hDAT, and Gly149 in hNET. Three rotations of the substrates around the longitudinal axis were identified. In each mode, an aromatic hydroxyl group of the substrates occupied equivalent volumes of the three binding pockets, where small changes in amino acid composition explains the differences in selectivity. Uptake experiments support that the 5-hydroxyl group of serotonin and the *meta*-hydroxyl group norepinephrine and dopamine are placed in the hydrophilic pocket around Ala173, Ser438, and Thr439 in hSERT corresponding to Gly149, Ser419, Ser420 in hNET and Gly153 Ser422 and Ala423 in hDAT. Furthermore, hDAT was found to possess an additional hydrophilic pocket around Ser149 to accommodate the *para*-hydroxyl group. Understanding these subtle differences between the binding site compositions of the three transporters is imperative for understanding the substrate selectivity, which could eventually aid in developing future selective medicines.

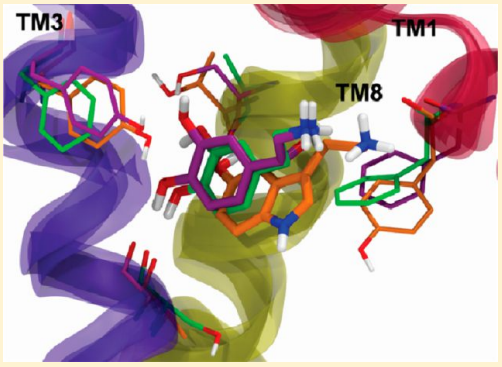

KEYWORDS: *Serotonin transporter, dopamine transporter, norepinephrine transporter, induced fit docking, molecular dynamics simulations, LeuT*

Monoamine transporters are secondary active transporters belonging to the neurotransmitter sodium symporter (NSS) family. From their location within the cell membranes of presynaptic neurons, they are responsible for reuptake of the biogenic monoamines serotonin (5-HT), dopamine (DA), and norepinephrine (NE) from the synaptic cleft after signaling. Malfunction of monoamine transporters has been shown to be involved in a variety of disorders such as depression, obsessive-compulsive disorder (OCD), Parkinson's disease, anxiety, attention deficit hyperactivity disorder (ADHD), and Tourette's Syndrome.[1] Accordingly, monoamine transporters are the target of a multitude of compounds, including antidepressants;[2−4] however, they are also the target of psychostimulants.[5−7] It is therefore of utmost importance to understand the function of this family of transporters from a pharmaceutical point of view. Unfortunately, no high resolution protein structure has been solved of the monoamine transporters so far, but with the availability of crystal structures of a bacterial homologue, the leucine transporter (LeuT) from *Aquifex aeolicus*, it has become possible to create homology models of hSERT, hDAT, and hNET and to predict the binding of substrates and inhibitors by molecular docking calculations.

Since the emergence of the first LeuT crystal structure with a leucine substrate bound,[8] 25 other crystal structures of LeuT have been deposited to www.pdb.org. These structures include LeuT with other amino acids bound,[9] LeuT containing detergent molecules in the extracellular site,[10] mutant LeuT structures used in electron paramagnetic resonance studies,[11] as well as LeuT with tricyclic antidepressant[12,13] and selective-serotonin inhibitors[14] bound. In addition to crystal structures of LeuT, the 3D structure of at least six other distantly related transporter families have been resolved by crystallography.[15−21] They all share the same overall topology, termed the "LeuT-fold", which means that they all contain an inverted repeat of

Received: September 6, 2012
Accepted: October 24, 2012
Published: October 24, 2012

Scheme 1. Chemical Structure of the Three Endogenous Monoamine Neurotransmitters Studied and Tyramine[a]

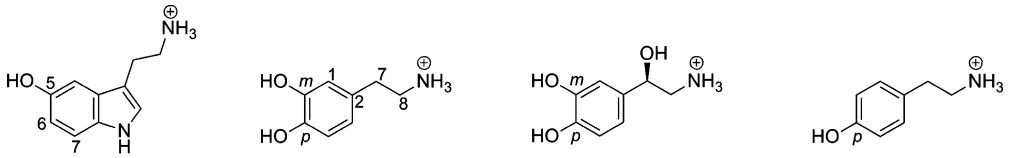

Serotonin (5-HT) Dopamine (DA) Norepinephrine (NE) Tyramine

[a]The serotonin substrate of hSERT with 5, 6, and 7 positions on the indole ring highlighted, the dopamine, DA, substrate of hDAT, and the *R*-norepinephrine, NE, substrate of hNET are also shown. For DA and NE, the *meta*- and *para*-hydroxyl positions are marked as is some of the identical atom numbering of DA and NE.

five transmembrane (TM) helices. These transporters are captured in different conformational states representing different stages of the transport cycle.

Most homology models of the monoamine transporters are constructed based on the first outward-occluded LeuT crystal structure,[8] which is in agreement with the finding that competitive inhibitors generally stabilize an outward-facing conformation.[22,23] Initially, some homology models resulting from either superpositioning of the neurotransmitter with leucine in LeuT[24] or from manual docking.[25] We have previously presented an experimentally validated binding model of 5-HT[26] in a hSERT homology model where the substrate is bound in a position similar to that of leucine in the central binding pocket of LeuT. In that study, different sequence alignments of hSERT to LeuT were included, and it was concluded that the comprehensive alignment published by Beuming et al.[24] produced the most reliable models of hSERT.[26] The computations resulted in two possible binding models of 5-HT differing in the rotation of the substrate around the longitudinal axis from the ammonium group to the 6-position of the indole ring; see Scheme 1. Through extensive structure−activity relationship (SAR) studies including hSERT mutants, one of the binding models was validated.[26] Shortly after this study, Kaufmann et al.[27] published a model of 5-HT binding to a homology model of the human and *Drosophila* SERT (dSERT),[27] also proposing two binding modes similar to the findings of Celik et al.[26] They, however, suggested a slightly different favorable binding mode of 5-HT compared to ours. Recently, we have published experimentally validated models of the binding of tricyclic antidepressants[28] and a serotonin selective reuptake inhibitor in hSERT[29] based on the alignment of Beuming et al.[24] A model of DA binding to rat DAT (rDAT) has been presented in a study by Indarte et al.,[30] which also included several sequence alignments and molecular docking schemes, though not the alignment proposed by Beuming et al.[24] Models of DA binding to hDAT have been published by Beuming et al.[31] which propose a binding model similar to the one for DA in rDAT. Homology models of hNET have appeared either in an *apo*-form[3,32] or with a bound NE introduced through simple superposition with the template ligand.[24] To the best of our knowledge, only one study addresses the binding of NE to hNET based on a automated docking simulation using a homology model of hNET based on LeuT as template.[33] However, this study does not focus on the binding of NE but rather on predicting side effects of known medicines by assessing the possible interaction of these with hNET. Finally, no directly comparative studies using the same methodology for studying the binding of the three monoamine neurotransmitters to their parent transporters have previously been published based on automated techniques.

As a logical extension to our hSERT homology model studies of the binding of substrate and inhibitors, we here present the results of the first directly comparable study on the existence of a common binding mode for the three monoamine neurotransmitters through comparative modeling of the human monoamine transporters, hSERT, hDAT, and hNET, and binding of their endogenous substrates in an occluded central binding pocket. The endogenous substrates were docked into their respective homology models in a consistent methodological manner allowing for comprehensive comparisons to be made. The computational studies reveal very important novel information regarding the similarities in binding pattern of the three substrates. To confirm the identified common binding mode for the three biogenic monoamines, a few selected uptake inhibition experiments were carried out using mutant transporters. Furthermore, MD simulations confirm that the proposed common binding mode is stable in all transporters. The results from the study provide knowledge also on differences in binding site composition between the transporters; such knowledge is important for designing future selective drugs targeting one or two of the three transporters only.

RESULTS AND DISCUSSION

Understanding of the similarities and subtle differences between the binding pockets of monoamine transporters and the possible similarities in substrate binding is of outmost importance in the understanding of selectivity between the transporters and in the further development of novel pharmaceuticals targeting one or more of the monoamine transporters. Here we extensively compare the amino acid composition of the substrate binding pockets of the three monoamine transporters based on homology modeling. Additionally, a common binding mode of the substrates in their corresponding transporters is proposed from computational chemistry methods combined with biochemically testing through uptake inhibition experiments.

Homology Modeling of hSERT, hDAT, and hNET. We have previously presented a homology model of hSERT based on the LeuT structure.[26] In this model nonmembrane embedded parts, especially EL2, were poorly organized due to a lack of template sequences in LeuT. This loop is located far away from the central primary binding pocket and is assumed to not affect binding studies. However, differential protease sensitivity of EL2 when substrates and inhibitors are bound [34] indicates that this assumption may be not be completely correct. Thus, we proceeded by optimizing these more distant parts of the protein including available structural and functional information regarding disulfide bridges,[35,36] secondary structure elements,[24] glycosylation sites,[37−40] and proteolysis sites[34] as

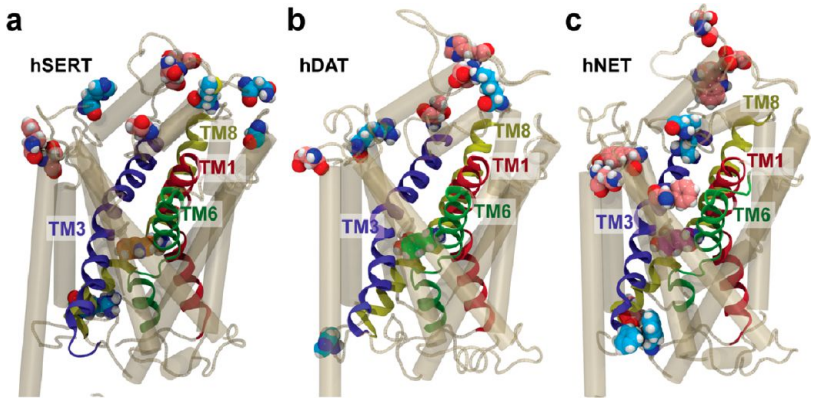

Figure 1. Location of residues identified from Ramachandran plots to be in disallowed and generously allowed regions. In all pictures, TM1 is shown in red, TM3 in blue, TM6 in lime, and TM8 in yellow. These four helices are the ones lining the central binding pocket. The remaining transmembrane helices (TM2,4,5,7,9−12) are shown in gray. (a) hSERT homology model with 5-HT bound (orange spheres). Residues in disallowed region, Asn205(EL2), His240(EL2), Ala305(EL3), Met389(TM7), and Arg462(TM9), are shown as cyan spheres. Residues in generously allowed region, Ser199(EL2), Asn211(EL2), Val397(EL4), Tyr572(TM12), and Ser574(TM12), are shown in pink spheres. (b) hDAT homology model with DA bound (green spheres). Residues in disallowed region, Arg237(EL2), Lys374(EL4), and His442(IL4), are shown as cyan spheres. Residues in generously allowed region, Thr173(EL2) His179(EL2), Asp191(EL2), and Asp555(EL6), are shown as pink spheres. (c) hNET homology model with NE bound (purple spheres). Residues in disallowed region, Phe133(IL1), Phe134(IL1), Val379(EL4), and Ala384(EL4), are shown as cyan spheres. Residues in generously allowed region, Trp173(EL2), Asp175(EL2), Thr200(EL2), His441(IL4), Tyr467(TM10), Phe540(EL6), and Asn555(TM12), are shown in pink.

described in Koldsø et al.[29] For modeling of the binding of the larger inhibitors in hSERT this refined homology model proved superior. Homology models of hDAT and hNET were built using a similar procedure by applying MODELLER[41,42] with the LeuT crystal structure and the optimized hSERT EL2 as templates utilizing the protocol from Koldsø et al.[29] This allows for a concurrent evaluation of the three human monoamine transporters focusing on similarities and differences. hSERT is included in this study to confirm that the previously published results are reproducible in this new and thoroughly refined homology model generated with novel versions of the software and to ensure a reasonable and fair comparison of the resulting models.

A total of 20 homology models were built for hDAT and hNET in MODELLER[41,42] and evaluated as described in the Methods while the most favorable hSERT model has previously been described.[29] Statistics of the 20 homology models is tabulated in the Supporting Information. All models show high percentages of populations of backbone dihedral angles in the "most favored" parts of the Ramachandran plots, and none can thus be excluded based on sterical features. Interestingly though, the models could be clearly separated into two groups when examining the rotamer state of the χ_1 dihedral angle of the conserved aspartic acid residue in the occluded binding site (Asp98 in hSERT, Asp79 in hDAT, and Asp75 in hNET). Approximately half of the models contain an *anti* rotamer state, while the required *gauche* rotamer state is observed in the remaining models. Only the latter conformation allows for the formation of the conserved interaction between the aspartic acid residue and the Na^+-ion occupying the Na1-site.[8,29,43] These models were then further evaluated, as described in Koldsø et al.[29] The main obstacle in introducing ligands into the occluded binding sites of the monoamine transporters seems to be the relatively small cavities of the homology models,[26] which are due to the small ligand binding site found in the template LeuT being occupied by the smaller leucine molecule. Thus, preferred models for each transporter were selected based on having as large as possible cavity size. Additionally, this binding site obstacle was overcome in the docking calculations by employing the induced fit docking method[44] where protein flexibility is indeed included in the docking protocol. Furthermore, Molpdfs as low as possible were used in the selection, hereby ensuring a more energetically favored relaxed protein. The selected model of hSERT has 89.5, 8.5, 1.0, and 1.0% populations in most favorable, additionally allowed, generously allowed, and disallowed regions, respectively, determined from a Ramachandran plot. Five residues Asn205(EL2), His240(EL2), Ala305(EL3), Met389(TM7), and Arg462(TM9) are located in the disallowed region (cyan spheres, Figure 1a), and five residues Ser199(EL2), Asn211(EL2), Val397(EL4), Tyr572(TM12), and Ser574(TM12) are located in the generously allowed region (pink spheres, Figure 1a). All of these 10 residues, however, are located more than 12 Å away from the substrate in the binding pocket and furthermore found at the surface of the protein or in loop-regions, and therefore do not necessarily need to show favorable values in a Ramachandran plot which reflects the secondary structure elements; see Figure 1a. The best model of hDAT has 90.8, 7.8, 0.8, and 0.6% populations in most favorable, additionally allowed, generously allowed and disallowed regions, respectively, as determined from the Ramachandran plot. Three residues, Arg237(EL2), Lys374(EL4), and His442(IL4), were found in the disallowed region (cyan spheres, Figure 1b), and four residues, Thr173(EL2) His179(EL2), Asp191(EL2), and Asp555(EL6), in the generously allowed region (pink spheres, Figure 1b). All seven residues are located more than 21 Å away from the substrate in the binding pocket in loop regions; see Figure 1b. The preferred model of hNET had 89.7, 8.1, 1.4, and 0.8% populations in most favorable, additionally allowed, generously allowed and disallowed regions, respectively, as determined from the Ramachandran plot. Four residues, Phe133(IL1), Phe134(IL1), Val379(EL4), and Ala384(EL4), were found in the disallowed regions (cyan spheres, Figure 1c), and seven residues, Trp173(EL2), Asp175(EL2), Thr200(EL2), His441(IL4), Tyr467(TM10), Phe540(EL6), and Asn555(TM12), in

the generously allowed regions (pink spheres, Figure 1c). All 11 residues are located more than 14 Å away from the substrate in the binding pocket placed either in loops or being surface exposed; see Figure 1c.

Ion Binding Sites in hSERT, hDAT, and hNET Homology Models. Common for hSERT, hDAT, and hNET are their dependence upon sodium and chloride ion gradients to facilitate the energetically demanding reuptake of their endogenous substrates. The stoichiometry these transporters use to transport substrate and ions are however different. hSERT has an overall electroneutal transport cycle, with a stoichiometry of 5-HT/Na^+/Cl^-/K^+ of 1:1:1:1, where Na^+ and Cl^- are co-transported, while K^+ is counter-transported.[45,46] The transport cycle of hDAT and hNET both result in net positive charge transfer, with stoichiometry of DA/Na^+/Cl^- being 1:2:1,[47] and NE/Na^+/Cl^- of 1:1:1.[47,48] Here no counter-transport of K^+ has been reported.[45] Amino acids forming the binding sites for the two sodium ions are highly conserved among the three monoamine transporters and their positions were resolved in the LeuT crystal structure. An additional binding site for a chloride ion is conserved in the chloride-dependent monoamine transporters.[49,50] The high degree of conservation of the sodium sites among the monoamine transporters and in LeuT is revealed in Table 1. Additionally, the residues lining the chloride ion binding site in the Cl^--dependent monoamine transporters are very similar to the corresponding ones of the Cl^--independent LeuT, in which the negative charge is harbored on Glu290.

Table 1. Residues Interacting with the Two Sodium and the Chloride Ions in LeuT and the Three Monoamine Transporters[a]

	LeuT	hSERT	hDAT	hNET
Na1	*leucine*	*Asp98*	*Asp79*	*Asp75*
	Ala22	Ala96	Ala77	Ala73
	Asn27	Asn101	Asn82	Asn78
	Thr254	Ser336	Ser321	Ser318
	Asn286	Asn368	Asn353	Asn350
Na2	Gly20	Gly94	Gly75	Gly71
	Val23	Val97	Val78	Val74
	Ala351	Leu434	Leu418	Leu415
	Thr354	*Asp437*	*Asp421*	*Asp418*
	Ser355	Ser438	Ser422	Ser419
Cl^- (not LeuT)	Tyr47	Tyr121	Tyr102	Tyr98
	Thr254	Ser336	Ser321	Ser318
	Asn286	Asn368	Asn353	Asn350
	Glu290	*Ser372*	*Ser357*	*Ser354*

[a]Major differences in residue properties are depicted in italic letters.

However, three significant differences in amino acid composition are observed between LeuT and the monoamine transporters, likely to be conferring the differences in ion dependencies. The main difference in the Na1-site is that the substrate carboxyl group interacting with the Na1-ion in the LeuT structure is replaced by an aspartic acid residue in the monoamine transporters (Asp98 in hSERT, Asp79 in hDAT, and Asp75 in hNET). This is a general substitution observed between amino acid transporters and monoamine transporters and is a classic example of the deletion model for receptors.[26,51]

In the Na2-site, the LeuT Thr354 residue is replaced by aspartic acid residues in the monoamine transporters. Contrary to LeuT, the monoamine transporters therefore have charged residues involved not only in Na1-ion coordination but also in coordination of the Na2-ion: Asp437 (hSERT), Asp421 (hDAT), and Asp418 (hNET) compared to Thr354 in LeuT. This specific residue has recently been shown to play a central role in Na2 transport in LeuT,[52] but also the corresponding Asp437 has been illustrated to be important in transport of the Na2-ion in hSERT.[53] It has been suggested that the electrostatics from the charged residue in Na1-ion coordination is important for selectivity.[54] The Na2 coordination was mostly dependent on "snug-fit" of proteins giving a binding pocket where geometric properties are dominant.[54,55] In the homology models of the monoamine transporters, the Na2-ion coordination is slightly distorted compared to the one observed in LeuT, due to the different side chain of an aspartic acid (monoamine transporters) compared to threonine (LeuT). Therefore, the Na2-site coordination and selectivity could possibly also be electrostatic, yielding a similar ion dependence and property of the Na1- and Na2-site in monoamine transporters, whereas two different properties, namely, "snug-fit" and electrostatic, of the sodium sites are speculated in LeuT by Noskov and Roux.[54,55]

The chloride binding site in the monoamine transporters stems from the substitution of Glu290 in LeuT for serine residues in the monoamine transporters; the presence of a negative species, either from an acidic protein residue or a chloride ion, in this vicinity was shown to be crucial for transport in monoamine transporters as illustrated by mutation of Ser372 in hSERT to an acid similar to Glu290 in LeuT, which induced a Cl^--independent transporter[49] and vice versa for Glu290Ser mutation in LeuT that became chloride dependent.[50]

IFD of 5-HT. As a check for consistency, the binding of 5-HT has been explored in the refined homology model with the optimized loops and compared to the previously published and experimentally validated models.[26] The IFD calculations using the new and refined homology model of hSERT resulted in 64 poses of 5-HT bound in the central cavity. The poses could be assigned to three clusters of binding, **5HT-1**, **5HT-2**, and 5HT-3, respectively; see Figure 2a–c. A population of 32 poses was observed in **5HT-1**, 22 poses in **5HT-2**, and 5 poses in **5HT-3**, as listed in Table 2. The two clusters **5HT-1** and **5HT-2** are similar to the ones previously observed by us[26] and others.[27] The coordination between the quaternary ammonium center of 5-HT and Asp98 of the binding site is found in all three clusters, and so is a hydrogen bond between the quaternary nitrogen atom and the backbone carbonyl group of Phe335 in the aromatic lid; see Figure 2a–c. The 6-position of the indole ring is pointing toward Ala173 and Ala169 in all three clusters (see Figure 2a–c), as previously validated by extensive SAR and mutagenesis studies.[26] Accordingly, the main difference between the three clusters of 5-HT stems from rotations around the long ligand axis. The position of the 5-hydroxyl (5-OH) group therefore differs between the three clusters. Hydrogen bonding interactions is observed with Ala169 (**5HT-1**), Ser438 (**5HT-2**), or Ile172 and Tyr175 (**5HT-3**); see Figure 2a–c. In the work of Celik et al.,[26] it was experimentally validated that the 5-OH group is pointing toward the hydrophilic pocket lined by Ser438 and Thr439. This strongly indicates that **5HT-2** is the correct binding mode. A later study by Kaufmann et al.[27] found binding modes of 5-HT resembling **5HT-1** and **5HT-2** in *Drosophila* SERT

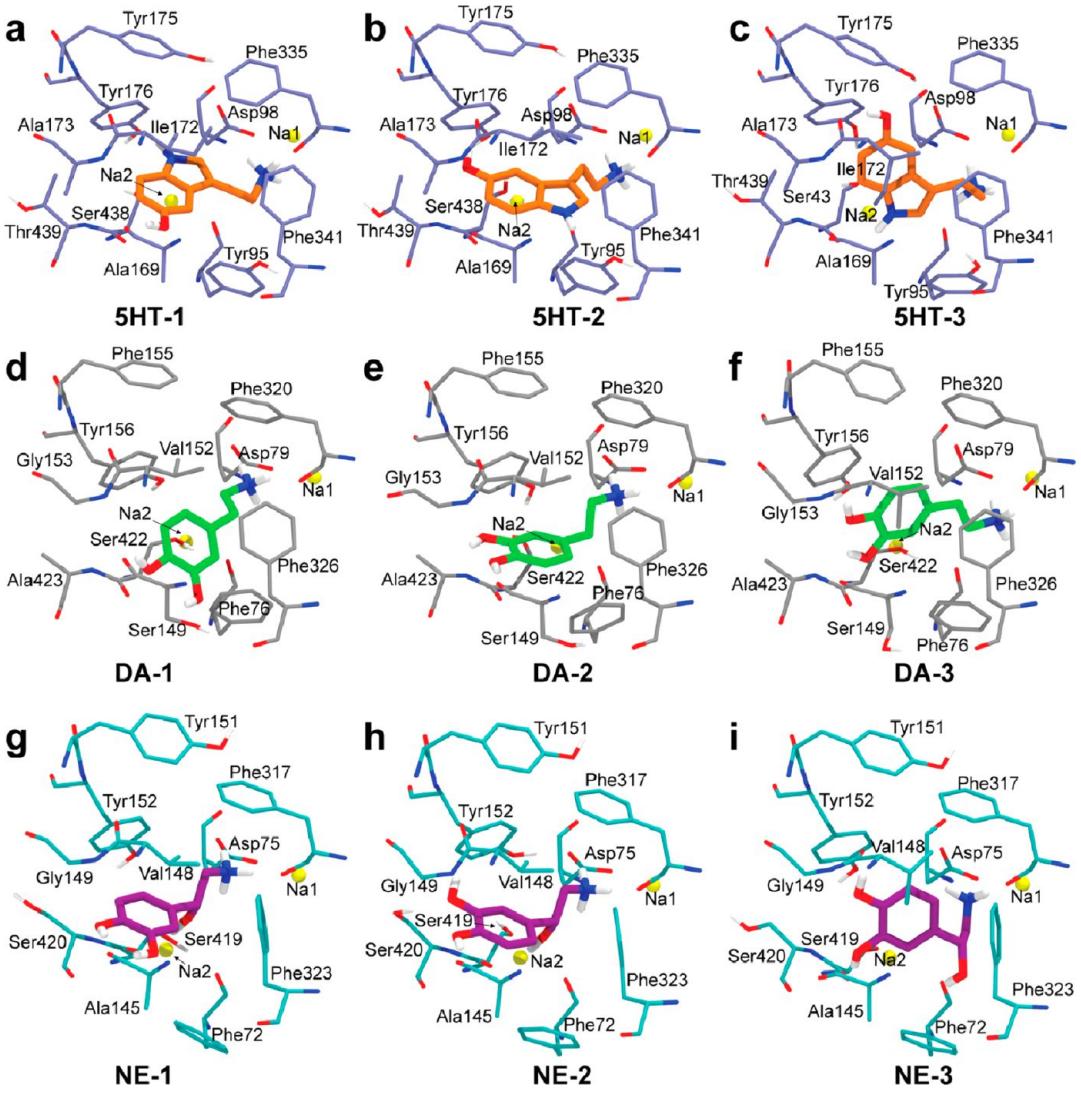

Figure 2. Binding modes of the endogenous substrates in their corresponding transporters. (a–c) hSERT binding site residues are shown in light blue, and 5-HT is colored by elements with orange carbons. The three pictures illustrate the three observed binding modes: (a) **5HT-1**, (b) **5HT-2**, and (c) **5HT-3**. (d–f) hDAT binding site residues are shown in light gray, and DA is colored by elements with green carbons. The three pictures illustrate the three observed binding modes: (d) **DA-1**, (e) **DA-2**, and (f) **DA-3**. (g–i) hNET binding site residues are shown in light blue, and NE is colored by elements with purple carbons. The three pictures illustrate the three observed binding modes: (g) **NE-1**, (h) **NE-2**, and (i) **NE-3**.

(dSERT). The conclusions were drawn from QSAR based on known data.[27]

IFD of DA. The IFD calculations resulted in 74 poses of DA in hDAT, and these poses could similarly to 5-HT be assigned into three clusters of binding, **DA-1**, **DA-2**, and **DA-3**; see Figure 2d–f. A population of 42 was observed in **DA-1**, 11 in **DA-2**, and 12 in **DA-3** (Table 2). The coordination between the quaternary nitrogen atom of DA and Asp79 of the binding site is present in all three clusters, and so is a hydrogen bond between the quaternary nitrogen atoms and the backbone carbonyl group of Phe320 in the aromatic lid analogous to what was observed in hSERT; see Figure 2d–f. As observed from the 6-position of 5-HT in hSERT, the aromatic hydroxyl group of DA positioned *para* to the ethylamine group (*para*-OH) points toward Ser149 in hDAT in **DA-1** and **DA-2**, with a displacement in **DA-3**; see Figure 2d–f. Accordingly, the longitudinal axis of DA in hDAT projects from Asp79 to Ser149. The orientation of the hydroxyl substituent *meta* to the ethylamine group (*meta*–OH) differs the most in the three clusters; see Figure 2d–f. In **DA-1** both the *meta*-OH group and *para*-OH groups form hydrogen bonds with Ser149 through the backbone carbonyl and the hydroxyl side chain; see Figure 2d. The ligand is rotated 180° around the longitudinal axis in **DA-2** compared to **DA-1**, positioning *meta*-OH for hydrogen bonding with the Ser422 backbone carbonyl (Figure 2e). Both **DA-1** and **DA-2** binding modes have previously been described by others.[30,31,56] In **DA-3**, the *para*-OH group forms a hydrogen bond with the backbone carbonyl of Val152 instead of Ser149 and the *meta*-OH group forms a hydrogen bond with the Ser422 backbone carbonyl (Figure 2f), hereby **DA-3** is the only binding mode of DA that does not interact directly with Ser149. Based on the number of poses obtained from the IFD, there seems to be a preference for **DA-1**, while **DA-2** is the cluster obtaining the most favorable GlideScore and Emodel. However, it is not possible to fully distinguish between these three binding modes solely based on the IFD calculations; therefore, biochemical experiments were undertaken (please see below) to determine the interaction partners of the substrate hydroxyl groups.

dx.doi.org/10.1021/cn300148r | *ACS Chem. Neurosci.* 2013, 4, 295–309

Table 2. Statistics for the Three Clusters Identified from Induced Fit Dockings of 5-HT, DA, and NE in hSERT, hDAT, and hNET[a]

protein	cluster	no. poses/ total poses	distance Asp98(Oδ)−N$^+$ (Å)	GlideScore (kcal/mol)	Emodel (kcal/mol)
hSERT	**5HT-1**	32/64	3.60 [0.90]	−7.1 [0.7]	−57.3 [6.5]
	5HT-2	22/64	3.01 [0.49]	−7.3 [0.8]	−58.7 [5.8]
	5HT-3	5/64	3.62 [0.51]	−7.3 [0.8]	−58.4 [3.9]
protein	cluster	no. poses/ total poses	distance Asp79(Oδ)−N$^+$ (Å)	GlideScore (kcal/mol)	Emodel (kcal/mol)
hDAT	**DA-1**	42/74	2.75 [0.20]	−8.3 [0.4]	−49.3 [3.0]
	DA-2	11/74	2.79 [0.20]	−8.7 [0.5]	−50.3 [3.7]
	DA-3	12/74	2.97 [0.27]	−8.3 [0.6]	−52.1 [5.0]
protein	cluster	no. poses/ total poses	distance Asp75(Oδ)−N$^+$ (Å)	GlideScore (kcal/mol)	Emodel (kcal/mol)
hNET	**NE-1**	26/78	2.76 [0.23]	−8.4 [0.7]	−59.4 [4.1]
	NE-2	40/78	2.76 [0.27]	−8.6 [0.6]	−58.8 [5.0]
	NE-3	6/78	2.91 [0.18]	−7.7 [1.0]	−55.5 [6.4]

[a]In the table, the protein binding mode has been listed in the cluster column, and the number of poses related to the total amount of poses. Additionally, the mean value is listed for the hydrogen bond distance with the conserved aspartic acid (Asp98 in hSERT; Asp79 in hDAT, and Asp75 in hNET), the GlideScore and Emodel. Please see the Methods for a description of the scoring functions. Standard deviations are shown in brackets.

IFD of NE. The IFD calculations resulted in 78 poses of NE in hNET, and these poses could similarly be divided into three clusters of binding, **NE-1**, **NE-2**, and **NE-3**; see Figure 2g–i. A total of 26 poses populates **NE-1**, 40 poses in **NE-2**, and 6 in **NE-3** (Table 2). Also for NE the coordination between the quaternary nitrogen atom of NE and Asp75 of the binding site is present in all three clusters, so is a hydrogen bond between the quaternary nitrogen atom and the backbone carbonyl group of Phe317 in the aromatic lid; see Figure 2g–i. In **NE-1** and **NE-2**, a hydrogen bond is observed between the *para*-OH group and Ala145, yielding the same longitudinal axis of NE as observed for DA and 5-HT; see Figure 2. In **NE-1**, a hydrogen bond is formed with the backbone of Ala145 through both the *meta*-OH and the *para*-OH groups, whereas the hydroxyl group at the ethylamine (2-OH) forms a hydrogen bond with Ser419 in 14 of the 26 poses, with Phe72 backbone in 9 of the 26 poses, and the remaining 3 poses interacts with the Asp98 carboxylate group; see Figure 2g. In **NE-2**, a hydrogen bond is formed with the side chain of Ser420 through the *meta*-OH group, while the 2-OH forms a hydrogen bond with the backbone carbonyl of Ser419 in 28 of the 40 poses, whereas the remaining 12 poses points toward the Phe72 backbone; see Figure 2h. In **NE-3**, the aromatic hydroxyl groups, *meta*-OH and *para*-OH, form hydrogen bonds with Ser419 and Val148, respectively, while 2-OH is positioned toward Phe72 in 4 of the poses, toward Ser419 and Phe317 in one pose each; see Figure 2i. Similarly to **DA-3** above, **NE-3** is the only binding mode not interacting with Ala145 (corresponding to Ser149 in hDAT). There seems to be a preference for **NE-2** based on the number of poses occupying the different binding modes of NE. This binding mode is also the one observed in a previous study.[33] A fair amount of poses is also observed in **NE-1**, indicating that this binding mode could also be of relevance. Again, the difference between binding mode 1 and 2 is the interaction partners for the two aromatic hydroxyl groups; this is assessed experimentally below.

Comparison of Substrate Binding Sites in hSERT, hDAT, and hNET Homology Models. The amino acid composition of the substrate binding sites has been compared between the three monoamine transporters and LeuT (Figures 3 and 4). It is evident that there is a high degree of conservation of the binding site amino acids between the bacterial and the mammalian transporters. When comparing the residues within 5 Å of the observed substrate binding sites, the identities between the bacterial LeuT and the human transporters are 54%, 46%, and 57% for hSERT, hDAT, and hNET, respectively. One of the most important substitutions between LeuT and the monoamine transporters is Gly24 in LeuT, which is an aspartic acid in the three other transporters (Asp98 in

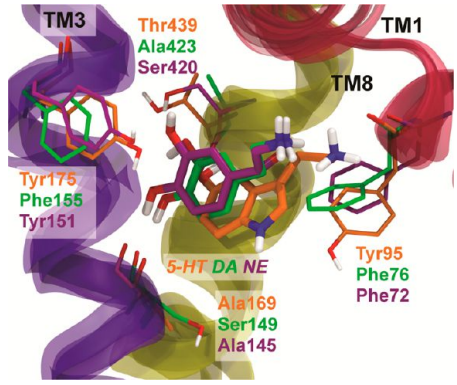

Figure 4. Residues in the central binding pocket differ between the transporters. TM1 is shown in red, TM3 in purple, and TM8 in yellow. 5-HT substrate (orange bold sticks) in the **5HT-2** binding mode has been shown together with hSERT residues (orange sticks). DA substrate (green bold sticks) in the **DA-2** binding mode has been shown together with hDAT residues (green sticks). NE substrate (purple bold sticks) in the **NE-2** binding mode has been shown together with hNET residues (green sticks).

LeuT	N21	A22	V23	G24	L25	G26	N27	I100	P101	L102	V104	A105	Y107	Y108	V109	F252	F253	T254	L255	S256	F259	I262	S355	S356	I357	A358	I359	M360
hSERT	*Y95*	A96	V97	D98	L99	G100	N101	I168	A169	F170	I172	A173	Y175	Y176	N177	F334	F335	S336	L337	G338	F341	V343	S438	T439	F440	A441	G442	L443
hDAT	F76	A77	V78	D79	L80	A81	N82	I148	*S149*	L150	V152	G153	*F155*	Y156	N157	C319	F320	S321	L322	G323	F326	V328	S422	*A423*	M424	G425	G426	M427
hNET	F72	A73	V74	D75	L76	A77	N78	I144	A145	L146	V148	G149	Y151	Y152	N153	F316	F317	S318	L319	G320	F323	V325	S419	S420	M421	G422	G423	M424

Figure 3. Overview of residues in the occluded binding site of the LeuT and the three monoamine transporters. The residues fully conserved between the four types of transporters are shown in dark blue. The residues conserved between three of the transporters are shown in middle blue, and the residues conserved between two transporters are highlighted pairwise as either light blue or light red. The nonconservative mutations within the monoamine transporters are indicated by italic letters and red boxes, whereas residues fully conserved between the three monoamine transporters are highlighted by green boxes.

dx.doi.org/10.1021/cn300148r | *ACS Chem. Neurosci.* 2013, 4, 295–309

Table 3. Mean K_i (μM) and 95% Confidence Intervals (in brackets) for Inhibition of [^{3}H]-DA from at Least Three Independent Experiments

	K_i (μM)					
	dopamine		norepinephrine		tyramine	
hDAT wt	6.65	[4.16−10.64]	18.66	[11.67−29.79]	6.28	[0.55−71.61]
hDAT S149A	6.75	[4.75−9.57]	25.6	[12.2−53.7]	4.03	[1.95−8.28]
hDAT S149V	10.19	[7.67−13.49]	38.3	[9.3−157.0]	9.23	[1.82−46.67]
hDAT S149T	2.23	[1.26−3.97]	13.71	[7.91−23.71]	1.069	[0.664−1.722]
hNET wt	0.925	[0.682−1.253]	3.35	[2.23−5.02]	0.454	[0.327−0.632]
hNET S419A	2.16	[1.30−3.59]	2.01	[0.66−6.17]	36.7	[13.34−101.16]
hNET S419V	3.49	[2.02−6.03]	2.51	[0.87−7.26]	79.4	[11.43−552.08]
hNET S419T	0.993	[0.575−1.718]	7.33	[2.74−19.59]	1.816	[0.713−4.624]
hNET S420A	0.671	[0.386−1.167]	2.08	[0.77−5.60]	0.476	[0.324−0.700]
hNET S420V	3.05	[2.09−4.45]	9.42	[1.66−53.46]	2.19	[0.84−5.69]
hNET S420T	1.191	[0.767−1.854]	5.13	[2.67−9.84]	0.348	[0.180−0.675]

hSERT, Asp79 in hDAT, and Asp75 in hNET). In this mutation, an acidic residue substitutes for the carboxylate group in leucine in LeuT with respect to the Na1-site. The identity within the monoamine transporters is even more pronounced; see Figure 3. hSERT shares an identity of 57% and 68% with hDAT and hNET, respectively, within the binding site. Additionally, the identity between hNET and hDAT is 86%. Only few of the substitutions between these transporters change the property of the residues. Worth noticing is the hSERT Tyr95, which is a phenylalanine in hDAT and hNET; see Figure 4. This residue has previously been observed to interact with selective hSERT ligands such as *S*-citalopram.[29,57,58] From the studies of *S*-citalopram, it could be observed that demethylation of the quaternary ammonium group caused a decrease in affinity.[29] This suggests that Tyr95 in hSERT favors dimethylated species, such as *S*-citalopram and imipramine, which can further be supported by the well-known selectivity of imipramine for hSERT and desipramine, with only one *N*-methyl group, for hNET with a phenylalanine at this position.[59,60] Accordingly, this residue can be speculated to be part of a hSERT selectivity filter favoring dimethylated species compared to hNET and hDAT. The comparable Phe76 in hDAT has been shown to form favorable interactions with the hydrophobic aromatic ring of the substrate DA.[31] In **NE-1** and **NE-2**, the 2-OH group of NE is interacting with the Ser419 backbone carbonyl and the aromatic ring of NE is thereby exposed in a similar way as found for DA in hDAT, and could possibly interact with Phe72 in hNET through hydrophobic and/or π-interactions. The **5HT-2** binding mode has the indole N−H pointing toward Tyr95 and could therefore interact by electrostatic interactions with the residue at this position. Thus, the difference in amino acid at this position between the three transporters is met by accompanying differences in the substrate functional groups, all being able to form a favorable interaction and this interaction may be an important part of the substrate selectivity filter. Indeed, Amara and co-workers[61] have shown that the conservative hSERT Y95F mutation is sufficient to confer robust DA uptake capacity to hSERT, albeit by means of a mechanistically different process.

Within the substrate binding site of hSERT a hydrophobic pocket was identified in the area around Ala169 and Ile172 while a hydrophilic pocket is present around Ser438 and Thr439.[26,28,29] Interestingly, when comparing the amino acid composition of the three monoamine transporters in the hydrophobic pocket, we see that hNET is very similar to hSERT with Ala145 and Val148 forming this pocket, however, hDAT contains a property changing substitution in this pocket and is composed of Ser149 and Val152. This change from an alanine in hSERT and hNET to a serine in hDAT changes the characteristics of this area of the binding pocket to be more hydrophilic. The hydrophilic pocket observed in hSERT is also a hydrophilic one in hNET with residues Ser419 and Ser420. Here the only difference is a serine in hNET instead of threonine in hSERT, which would not change the electrostatic properties much but rather result in differences in binding site volume and hereby may be involved in substrate selectivity. In contrast, the corresponding residues in hDAT are Ser422 and Ala423; see Figure 4. Here the hydrophilic pocket in hDAT is therefore more hydrophobic compared to hSERT and hNET. The hDAT binding pocket clearly encompasses some different properties compared to hSERT and hNET, since it contains two mixed hydrophilic/hydrophobic pockets instead of one hydrophilic and one hydrophobic. Based on this, it could be favorable for the two hydroxyl groups of DA to be orientated in either of the pockets. Thus, it can be speculated that the DA substrate can be bound with more degrees of freedom within the central binding site of hDAT.

Another property changing difference in amino acid composition between the three transporters is the Tyr175 and Tyr151 in hSERT and hNET, respectively, which is Phe155 in hDAT. This difference in amino acid composition between hSERT and hDAT has recently been shown to be involved in the difference in selectivity of mazindol and analogue binding (unpublished data). Phe155 of hDAT, Tyr175 of hSERT, and Tyr151 of hNET are located next to the aromatic lid, and the difference in property of this residue could possibly function as a selectivity filter just above the central binding pocket before substrate or other ligands enter the binding pocket.

Biochemical Exploration of Binding Modes. Based on the binding modes predicted from the IFD calculations, we performed single-point mutations in the area in which the binding pockets of the monoamine transporters differ most; see Table 3. To explore the binding of DA we constructed hDAT mutants where the binding pocket around Ser149 of hDAT was converted into a similar site as observed in hSERT and hNET. hDAT Ser149 appears important for the coordination of the *para*-OH present in DA from the docking calculations, and could accordingly also be important for binding of *para*-OH of NE and tyramine; see Scheme 1. We would expect that mutating this residue would result in a similar pattern in affinity toward hDAT for all three substrate analogues, however, most

pronounced for tyramine which carries fewer potential hydrogen bonding groups than DA and NE and thus should be most sensible to mutation of this residue. The hDAT Ser149Val mutation resulted in a approximately 2-fold loss in affinity of DA (hDAT wt K_i = 6.65 μM and hDAT Ser149Val K_i = 10.19 μM, p = 0.0436), which could indicate that the conversion from a hydrophilic site to a hydrophobic site in this area of the binding pocket has influence on DA binding. This is further evident from the 4-fold regain of affinity observed when reintroducing a hydrophilic residues by the hDAT Ser149Thr mutation (hDAT Ser149Val K_i = 10.3 μM and hDAT Ser149Thr K_i = 2.23 μM, p = 0.0002). Though not statistically significant, an identical pattern is observed for NE binding; when mutating hDAT Ser149 to valine the affinity decreases 2-fold (hDAT wt K_i = 18.66 μM and hDAT Ser149Val K_i = 38.2 μM) and increases 3-fold when reintroducing the hydrogen bonding potential (hDAT Ser149Val K_i = 38.2 μM and hDAT Ser149Thr K_i = 13.71 μM). As expected the relative gain of affinity when reintroducing the hydrogen bonding residue (Ser149Thr) instead of the hydrophobic mutants (Ser149Val) is most pronounced for tyramine with a 9-fold gain (hDAT Ser149Val K_i = 9.23 μM and hDAT Ser149Thr K_i = 1.069 μM, p = 0.0067). Taking together, hDAT Ser149 appears to participate in hydrogen bonding with a substrate moiety common to DA, NE and tyramine, that is, the *para*-OH as is observed in the **DA-1**, **DA-2**, **NE-1**, and **NE-2** binding modes.

The Ser420Val mutation in hNET causes the hydrophilic pocket of this transporter to become more hydrophobic similar to what is observed in hDAT and results in a 3-fold decrease in affinity of DA compared to wt hNET (hNET wt K_i = 0.925 μM and hNET Ser420Val K_i = 3.05 μM, p = 0.0001). This could be a result of hNET now containing two hydrophobic pockets, and thereby not providing a binding pocket for the *meta*-OH of DA. The lost affinity of DA can however be almost fully regained since the DA affinity of hNET Ser420Thr increases 3-fold by reintroducing a hydrophilic residue in this pocket (hNET Ser420Val K_i = 3.05 μM and hNET Ser420Thr K_i = 1.191 μM, p=0.002). Additionally, mutation of Ser419 in hNET to hydrophobic residues results in 2-fold (hNET wt K_i = 0.925 μM and hNET Ser419Ala K_i = 2.16 μM, p = 0.0041) and 4-fold (hNET wt K_i = 0.925 μM and hNET Ser419Val K_i = 3.49 μM, p = 0.0004) decrease in DA affinity for hNET, whereas the conservative Ser419Thr mutation in hNET does not affect DA affinity. These findings of a preference for a hydrophilic residue further suggest that the *meta*-OH of DA in hNET is located in this binding pocket lined by Ser419 and Ser420. Thus, the biochemical results suggest that DA is located as predicted in the **NE-2** binding mode.

A change from hNET Ser419Val to the hydrophilic hNET Ser419Thr resulted in a 4-fold gain in affinity for DA (hNET Ser419Val K_i = 3.49 μM and hNET Ser419Thr K_i = 0.993 μM, p = 0.002). In contrast, we observe the opposite change in NE affinity. The NE affinity for hNET Ser419Thr decreases 3-fold relative to the hNET Ser419Val mutation (hNET Ser419Val K_i = 2.51 μM and hNET Ser419Thr K_i = 7.33 μM, p = 0.057) indicating NE binding is negatively impacted by a more hydrophilic environment near hNET Ser419. The comparison of valine and threonine mutations rules out any major sterical differences with the hydrogen bonding potential being the dominating difference between these two residues. The only structural difference between DA and NE is the additional hydrogen bonding potential of the 2-OH so how this conflicts with the similarly added hydrogen bonding potential of hNET Ser419Thr is not immediately obvious. One possible explanation could be that the Ser419Thr mutation holding the Na2-coordination forces the methyl group of the introduced threonine to point toward the substrate as observed previously in hSERT.[62] This extra methyl group of the protein could therefore cause a steric clash with the 2-OH group of NE which is the major difference between DA and NE. However, we note that in both binding modes **NE-1** and **NE-2** the 2-OH group is found in proximity of hNET Ser419 in most of the poses from the docking calculations, suggesting that in hNET an unfavorable interaction can occur between the NE 2-OH group and hNET Ser419Thr. These findings indicate that both of the binding modes may account for NE binding. Additionally, the mutations of Ser420 to more hydrophobic residues result in decreased affinity of NE, whereas the Ser420Thr mutation results in a regain of some of the lost affinity. This clearly indicates that there is a preference for hydrophilic residues in the hydrophilic pocket of hNET, in line with the *meta*-OH of NE pointing toward Ser420, while the 2-OH group of NE is located in proximity of Ser419 in hNET. These observations points to **NE-2** as the most likely binding mode of NE.

Even though tyramine has an affinity for wt hDAT and wt hNET that is comparable to DA, the affinity of tyramine is affected much more than DA by a mutation that transforms hNET Ser419 to a hydrophobic residue. For example, the hNET Ser419Val mutant exhibits a staggering 175-fold loss of affinity for tyramine compared to hNET wt (hNET wt K_i = 0.454 μM and hNET Ser419Val K_i = 79.4 μM, p < 0.0001), whereas the same mutation causes only a 4-fold loss of affinity for DA (hNET wt K_i = 0.925 μM and hNET Ser419Val K_i = 3.49 μM, p = 0.0004). This is achieved without simultaneously affecting NE potency. Thus, the Ser419Val mutation eliminates the DA selectivity of hNET and reverses the selectivity for tyramine over NE. The relatively modest loss of affinity for the dihydroxylated DA compared to the dramatic loss of affinity for the monohydroxylated tyramine that is effected by the Ser419Val mutation shows us that the single hydroxyl group in tyramine is much more important in establishing stable hydrogen binding to hNET Ser419 than the similar hydroxyl of the more versatile catechol, DA, where presumably the neighboring *meta*-hydroxyl may substitute for this interaction if it is lost by mutation of Ser419 to valine.

Molecular Dynamics Simulations. To further investigate some of the conclusions drawn from the biochemical experiments, we performed MD simulations to probe the apparent stability of the different binding modes of DA and NE. Extended MD simulations have previously been carried out for the biochemically validated binding mode of 5-HT,[53] and they revealed that the substrate of hSERT remains stable in the **5HT-2** binding mode throughout five repeated 100 ns MD simulations of a dimer system. This further supports **5HT-2** as the correct binding mode of serotonin. MD simulations were initiated from hDAT containing DA both in the **DA-1** and **DA-2** binding modes. A similar approach was carried out for hNET, yielding four novel MD systems, namely, Sim(**DA-1**), Sim(**DA-2**), Sim(**NE-1**), and Sim(**NE-2**). Only binding modes 1 and 2 were investigated for DA and NE binding in hDAT and hNET, respectively, since binding mode 3 was rejected based on biochemical data. As discussed above, hDAT encompasses two mixed hydrophilic/hydrophobic pockets. In combination with DA being relatively small, it can be speculated that DA is more flexibly bound in the binding pocket than what is observed for

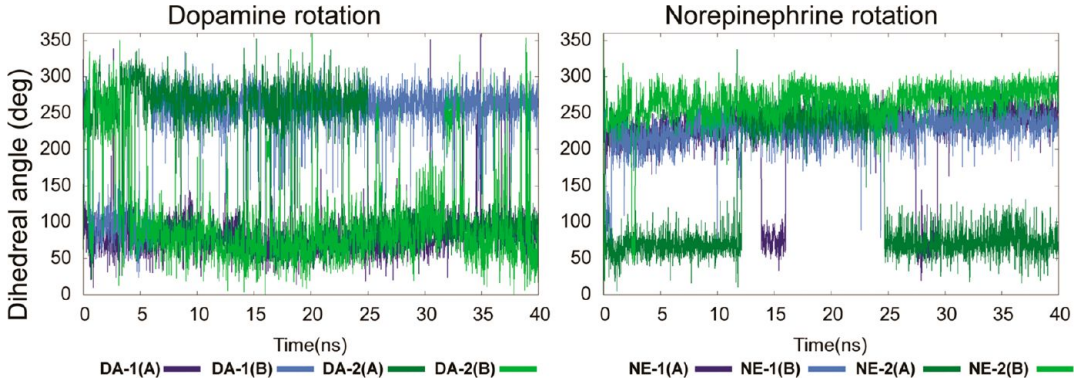

Figure 5. Rotation of the ligand within the binding pocket during simulation. The rotation angle was defined as the dihedral angle between C1−C2−C7−C8 (See Scheme 1). Left: Rotation of DA in Sim(**DA-1**) within the two monomers of hDAT chain A and B in dark and light blue, respectively. Rotation of DA in Sim(**DA-2**) is shown in dark green and light green for chain A and B respectively. Right: Rotation of NE in Sim(**NE-1**) within the two monomers of hNET chain A and B in dark and light blue, respectively. Rotation of NE in Sim(**NE-2**) is shown in dark green and light green for chain A and B, respectively.

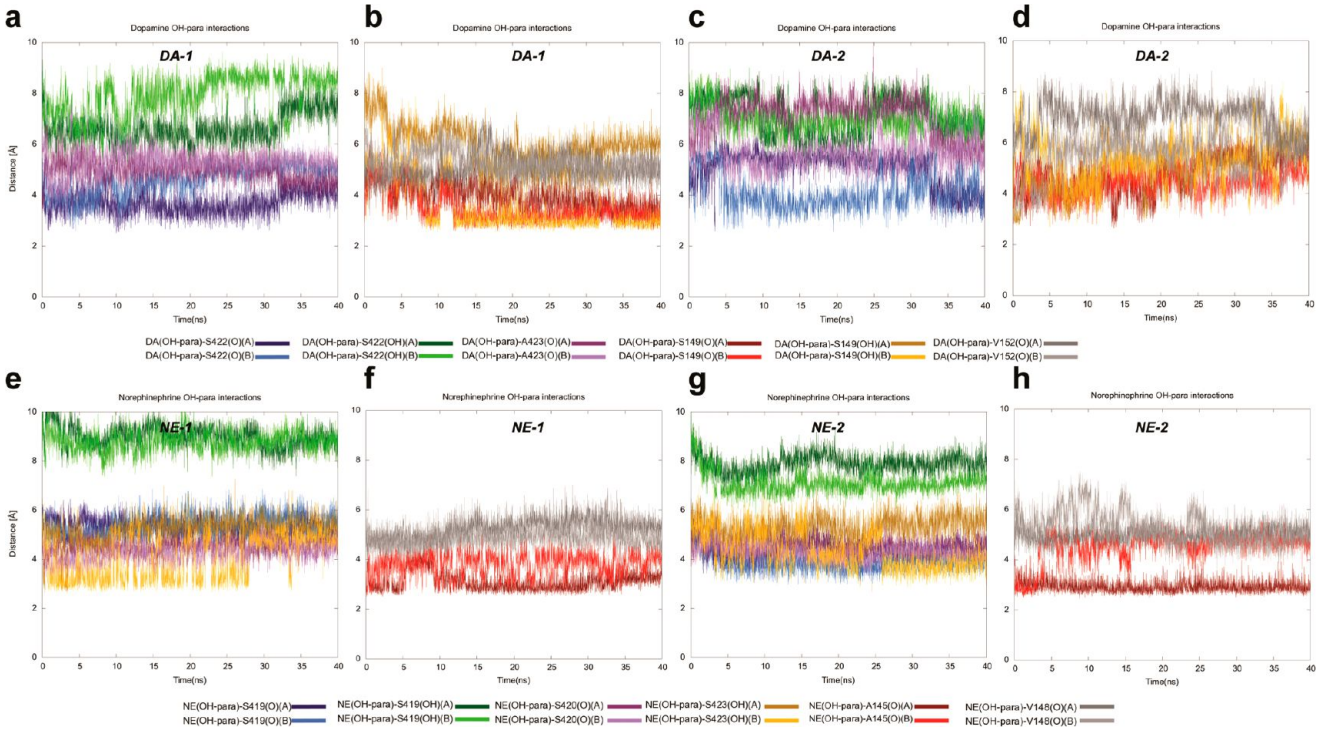

Figure 6. Interactions between *para*-OH of DA and NE and the hydrophilic and hydrophobic pockets. The dark color represents chain A, while the lighter color represent chain B. (a−d) *para*-OH DA interactions. Ser422(O) is shown in blue, Ser422(OH) is shown in green, A423(O) is shown in purple, S149(O) is shown in red, Ser149(OH) is shown in yellow, and V152(O) is shown in gray. The plots are divided into hydrophilic (a+c) and hydrophobic pockets (b+d), and **DA-1** is shown in (a) and (b) while **DA-2** is shown in (c) and (d). (e−h) *para*-OH NE interactions. Ser419(O) is shown in blue, Ser419(OH) is shown in green, S420(O) is shown in purple, Ser420(OH) is shown in yellow, A145(O) is shown in red, and V148(O) is shown in gray. The plots are divided into hydrophilic (a+c) and hydrophobic pockets (b+d), and **NE-1** is shown in (e) and (f) while **NE-2** is show in (g) and (h).

5-HT or NE in their respective transporters. hNET contains one hydrophilic and one hydrophobic pocket, and both the docking calculations and the biochemical experiments indicated that the *meta*-OH of NE would be located in the hydrophilic pocket lined by Ser420 and Ser421. The flexibility of the ligand inside the binding pockets was assessed from the simulation trajectories, and the results are depicted in Figure 5. It is clearly seen that DA fluctuates a lot inside both monomers of hDAT in the two binding modes sampled. Whereas both NE binding modes seems to remain more or less stable in the *−gauche* conformation of the C1−C2−C7−C8 dihedral angle (see atom numbering in Scheme 1; same numbering for DA and NE is used). Several changes are observed for DA between the *+gauche* to *−gauche* conformation of this dihedral angle, whereas only binding mode 2 of NE in chain A, **NE-2** (A), is seen to change from *+gauche* to *−gauche* after ∼12 ns of simulation where it then remains for ∼15 ns before it flips back again. This indicates that DA is more flexible than NE when bound to their cognate transporters.

The interactions between *para*-OH in both DA and NE were similarly followed during simulation (Figure 6). The *para*-OH group from both Sim(**DA-1**) and Sim(**DA-2**) is located

dx.doi.org/10.1021/cn300148r | *ACS Chem. Neurosci.* 2013, 4, 295−309

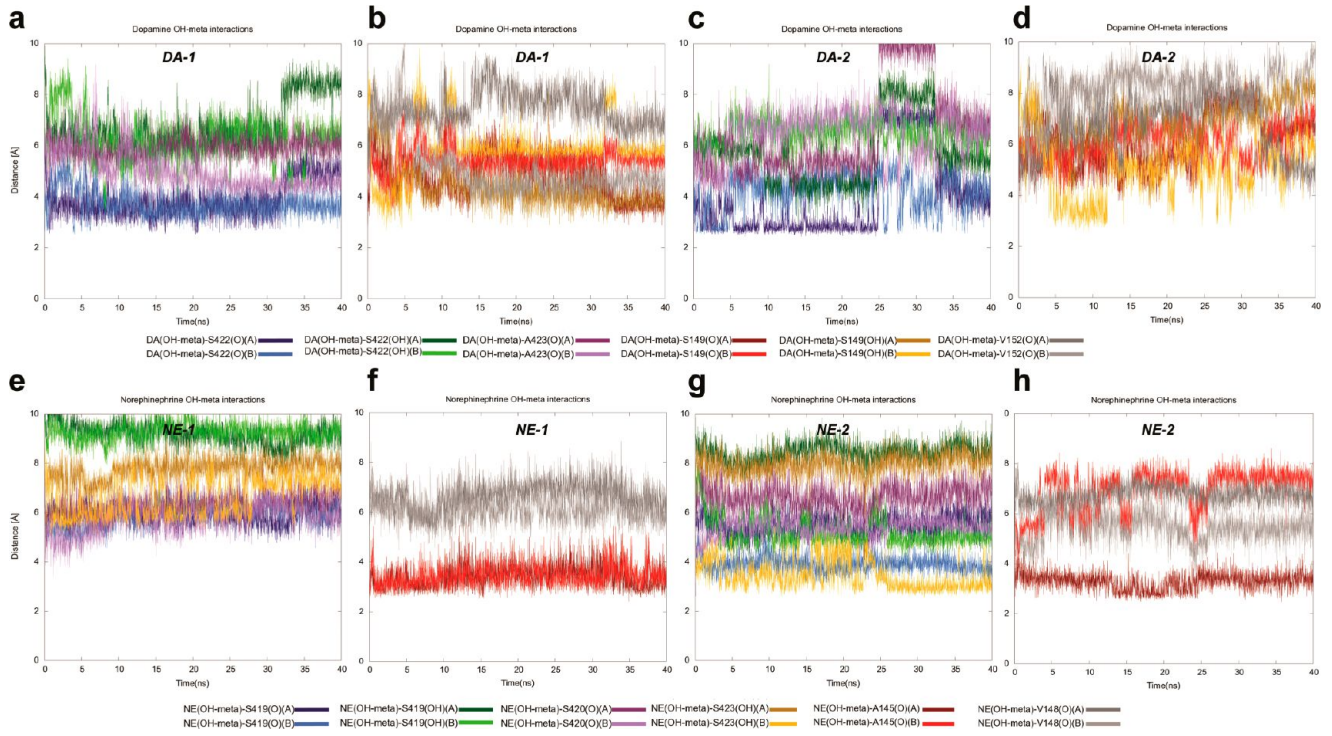

Figure 7. Interactions between *meta*-OH of DA and NE and the hydrophilic and hydrophobic pockets. The dark color represents chain A, while the lighter color represent chain B. (a–d) *meta*-OH DA interactions. Ser422(O) is shown in blue, Ser422(OH) is shown in green, A423(O) is shown in purple, Ser149(O) is shown in red, Ser149(OH) is shown in yellow, and Val152(O) is shown in gray. The plots are divided into hydrophilic (a+c) and hydrophobic pockets (b+d), and **DA-1** is shown in (a) and (b) while **DA-2** is show in (c) and (d). (e–h) *meta*-OH NE interactions. Ser419(O) is shown in blue, Ser419(OH) is shown in green, Ser420(O) is shown in purple, Ser420(OH) is shown in yellow, Ala145(O) is shown in red, and Val148(O) is shown in gray. The plots are divided into hydrophilic (a+c) and hydrophobic pockets (b+d), and **NE-1** is shown in (e) and (f) while **NE-2** is show in (g) and (h).

between the hydrophilic (See Figure 6, panels a and c) and the hydrophobic (Figure 6, panels b and d) pockets, interacting most closely with Ser422 and Ser149. In contrast, the *para*-OH group of Sim(**NE-1**) and Sim(**NE-2**) is located more toward the hydrophobic pocket lined by Ala145 often forming a hydrogen bond with the backbone carbonyl of this residue. From Figure 7, it is evident that binding mode **NE-2** more frequently forms hydrogen bonds to the transporter from the two aromatic hydroxyl groups than in binding mode **NE-1** (Figure 6, panels e–h).

The *meta*-OH interactions are the ones that most clearly differentiate between binding mode 1 and 2 of both DA and NE, as described in Figure 7. The *meta*-OH group within both Sim(**DA-1**) and Sim(**DA-2**) shows a preference for interactions with the Ser422 resembling the hydrophilic pocket in hSERT and hNET. This means that *meta*−OH of **DA-1** rotates during the initial part of the simulation from forming an interaction with Ser149 to interacting with Ser422. Combined it seems that the two binding modes of DA can acquire about the same number of hydrogen bonds. The *meta*-OH group of Sim(**NE-1**) show stable interactions with Ala145(O) in both chains during the entire simulation. On the other hand, the *meta*-OH group of Sim(**NE-2**) remains stable in chain B during the simulation, whereas the *meta*−OH group in chain A changes interaction partner from being Ser419 to Ala145(O). In total, the figures reveal that the binding mode **NE-2** engages more easily in hydrogen bonding with the residues of the transporter, pointing toward this binding mode as more favorable for NE.

In conclusion, the MD simulations thus further support the finding from the docking calculations, binding site comparisons and biochemical experiments. DA is a slightly smaller ligand than the others and hDAT contains two hydrophilic pockets which enables DA to fluctuate considerable more inside the binding pocket of the transporters. NE binding is proposed to be more stable based on the MD simulations. This observation together with the experiments allow us to believe that DA can adapt both binding mode **DA-1** and **DA-2**, while NE binds to hNET in the **NE-2** binding mode.

In this study, we have shown that 5-HT, DA, and NE share a common binding mode in the central binding pockets of their transporters. The 2-OH group of NE makes an interaction with the hNET Ser419 backbone carbonyl in a similar way as 5-HT forms a hydrogen bond via the 5-OH group to the corresponding residue Ser438 in hSERT, while DA forms interactions with Ser422 in hDAT via the *meta*-hydroxyl group of DA. The *para*-OH of NE is interacting with hNET Ala145 in both clusters **NE-1** and **NE-2**, whereas the *meta*-OH is the major difference between these two modes, interacting either with hNET Ala145 backbone or with Ser420 side-chain hydroxyl group or the backbone carbonyl. The hDAT binding pocket is observed to differ a little from the ones in hSERT and hNET, since two hydrophilic pockets are present. The *meta*- and *para*-OH groups can either interact with hDAT Ser149 through the side chain or backbone or with Ser149 backbone and Ser422 backbone. There seems to be a small preference for **DA-1** in hDAT based on the number of IFD poses, whereas biochemical experiments are most consistent with **DA-2**. It is also likely that **DA-2** is the preferred binding mode in hNET based on single-point mutational studies, though **DA-1** cannot be ruled completely out. This higher degree of flexibility within

dx.doi.org/10.1021/cn300148r | *ACS Chem. Neurosci.* 2013, 4, 295–309

the central binding pocket of DA could be a result of two hydrophilic pockets, and moreover, DA is an almost symmetric molecule in the sense that the ammonium and the two hydroxyl groups are the only possible specific anchoring partners within the binding pocket. Therefore, the difference between a displacement and a 180° rotation as observed between **DA-1** and **DA-2** is difficult to capture, and DA could possibly adopt different binding modes depending on the transporter to which it is bound. This can also be illustrated from the study by Beuming et al.[31] where actually all the hydroxyl group interactions in **DA-1** and **DA-2** are observed from the molecular dynamics simulations.

To summarize, three possible binding modes were found from docking simulations for each of the three neurotransmitters. In the binding mode classified as cluster 1, the 5-OH group in **5HT-1**, the *meta*-OH group in **DA-1**, and the *meta*-OH group in **NE-1** are positioned similarly in their respective binding pockets in the parent transporters with possible protein−ligand interaction points established to Ala169 in hSERT, Ser149 in hDAT, and Ala145 in hNET. Similarly in cluster 2, where **5HT-2**, **DA-2**, and **NE-2** show the same position of the hydroxyl group in 5-HT, and the *meta*-OH groups in DA, and NE forming hydrogen bonds to Ser438 in hSERT, Ser422 in hDAT, and Ser420 in hNET. The final cluster places the hydroxyl group in **5HT-3**, the *para*-OH group of **DA-3**, and **NE-3** toward Ile172 in hSERT, Val152 in hDAT, and Val148 in hNET, respectively. The results suggest there are three overall binding modes of substrates in the central cavity. Previous studies of DA binding in hDAT propose either **DA-1**[31] or **DA-2**[30,31,56] as being the most favorable based on homology modeling, docking, molecular dynamics, and mutagenesis. Similarly, we have suggested **5HT-2** to present the most likely binding mode of serotonin in hSERT,[26] whereas others have proposed **5HT-1** as the most likely binding mode.[27] The binding modes observed in this study for NE suggest that **NE-1** and **NE-2** are both likely but the experimental data and to a minor extent the MD simulations indicate a preference for a hydrophilic moiety in the pocket surrounded by Ser420, supporting the **NE-2** binding mode. Since the only difference between DA and NE is the 2-hydroxyl group attached at the ethylamine group, the extra hydrogen bond observed for NE could indicate that this substrate binds stronger in hNET. However, the affinity for NE is about 3-fold lower than for DA in both wt hNET and hDAT, suggesting that the 2-OH group does not contribute significantly to binding.

We have found that biochemical data is consistent with cluster 2 for all three transporters. If assuming that the substrates bind to the transporters using a common binding mode, there could be a preference for **DA-2**, **NE-2**, and **5HT-2**, since these have been biochemically validated via site-directed mutagenesis studies. These three binding modes of the substrates all have one hydroxyl group pointing into the hydrophilic pocket lined by Ser438 and Thr439 in hSERT; Ser422 and Ala423 in hDAT; and Ser419 and Ser420 in hNET.

Since development of new medications targeting the monoamine transporters must be predictable in relation to the selectivity in binding affinities toward the individual monoamine transporters, structural knowledge of the composition of the binding cavities in the three related transporters are of utmost need. Previously, substrates as amphetamine have inspired in the development of drugs; thus, comparative knowledge of the binding and orientation of the three monoamine neurotransmitters in their cognate transporter is imperative. The evaluations presented in this paper suggest that the three monoamine neurotransmitters bind similarly in their respective transporter and thus selectivity experienced among the biogenic amines for the three transporters is a very delicate question of establishing the correct contacts. We expect such knowledge to be extremely valuable for future development of ligands with a tailored selectivity profile for the transporters. Based on the studies presented here, we clearly observe that the binding of 5-HT and NE is specific, while DA binding seems to be much more promiscuous given the smaller size of the substrate but also because of the hDAT binding site being less clearly divided into different properties. This does indicate that hSERT and hNET selective ligands could take advantage of the hydrophilic and hydrophobic interaction pockets in different areas of the binding pocket. Possible hDAT selective inhibitors could then be similar in nature to DA taking advantage of the two hydrophilic pockets, but possibly be larger in size to freeze the interactions more than what is observed for DA. Virtual screening for new compounds that inhibit one of the transporters has been successful using homology models as described in an excellent recent review,[63] and we foresee that future design of compunds with tailor-made selectivities toward some of the monoamine transporters will be made possible through virtual screening and pharmacophore modeling using these comparable homology models of the transporters in an outward-occluded conformation. Although a lot still remains to be fully understood in relation to the similarities and differences between the closely related monoamine transporters, this high resolution comparison allow us to move one step closer.

METHODS

Model Preparation. Homology models of the three monoamine transporters were built in MODELLER 9v5[42] using the crystal structure of LeuT (PDB entry code 2A65)[8] as template and the alignment from Beuming et al.[24] in addition to an optimized extracellular loop 2 (EL2) of hSERT as described in Koldsø et al.[29] For all three monoamine transporters, 20 models were built and evaluated with respect to their molecular probability density function (Molpdf), the volumes of the occluded binding sites calculated in Molegro Virtual Docker,[64] and sterical features evaluated by Ramachandran plots calculated in PROCHECK.[65] Additionally, the χ_1 angle of the conserved aspartic acid in TM1, Asp98 (hSERT), Asp79 (hDAT), and Asp75 (hNET), should be ±*gauche* to establish the sodium coordination.[8] This angle has previously been proposed to be approximately ±65° in homology models of hSERT with bound *S*-citalopram.[29,43]

Two sodium ions were included in the binding sites corresponding to the coordinates observed in the crystal structure of LeuT (Na1 and Na2). The chloride ion was introduced in the suggested chloride binding site.[49,50] The homology models of the *apo*-monoamine transporters were minimized for 10 000 steps with a conjugate gradient algorithm in NAMD2.6[66,67] employing the CHARMM 27 force field[68] with the CMAP correction.[69,70] Data on all 20 models of each transporter can be seen in the Supporting Information.

Ligand Preparation. 5-HT, DA, and NE were built in Maestro 8.5[71] and minimized with a conjugate gradient algorithm until convergence followed by a conformational search in MacroModel 9.6[71] employing the OPLS-AA force field[72] in implicit water.

Induced Fit Docking. The Induced Fit Docking (IFD) protocol[44] from Schrödinger Inc., including Glide 5.0 and Prime 2.0,[71] was applied saving up to 100 poses and with an energy window of 50 kcal/mol. The ligand global minima structure was used as input. The binding site in hSERT was defined from Asp98 and Ile172.[26,28] Similarly, the corresponding residues in hDAT (Asp79 and Val152) and hNET (Asp75 and Val148) were employed. The SP docking[73] was applied in the initial docking stage of the IFD protocol, while the XP

Glide docking[74] was used in the redocking stage. The GlideScore is an empirical scoring function that accounts for the interaction energy between the ligand and the protein and approximates the ligand binding free energy while the Emodel score is a combination of the GlideScore, the nonbonded interactions, and the internal strain of the ligand.[73] Statistics and the full output are tabulated in the Supporting Information.

Molecular Dynamics (MD) Simulations. The binding mode of 5-HT previously biochemically validated by us has further been studied in Koldsø et al.[53] The **5HT-2** binding mode remains stable during 5 times 100 ns of simulations. The MD simulations of DA and NE in hDAT and hNET respectively have not previously been described by us; however, the simulation setup is similar to the one in Koldsø et al.[53]

Since the binding mode represented by cluster 3 could be discarded based on low population form calculations and from biochemical data, two protein−ligand complexes were used for both hDAT and hNET: Sim(**DA-1**), Sim(**DA-2**), Sim(**NE-1**) and Sim(**NE-2**).

All the protein−ligand complexes were simulated as a dimer similarly to the crystallographic structure of LeuT.[8] This gives two monomers for each system to analyze. The protonation states of ionizable residues were determined by PROPKA 2.0,[75] resulted in Glu396 and Glu491 being protonated; His223, His225, and His44 were modeled as histidinium, His165, His193, His228, His375, His442, and His547 were represented as the δ-tautomer, while His179 was modeled as the ε-tautomer for the two hDAT systems. Similarly, Asp418 and Glu488 was protonated whereas His222, His370, and His372 were modeled as histidinium, His199, His228, His296, His381, and His441 as the δ-tautomer ,and His280 as the ε-tautomer for the hNET systems. The systems were inserted into a pre-equilibrated ∼100 × 130 Å 1-palmitoyl-2-oleoylphosphatidylcholine (POPC) bilayer created by the membrane builder in VMD.[76] The system was solvated with the TIP3P[77] water model and afterward neutralized with NaCl to a concentration of 200 mM.

All simulations are performed in NAMD2.6[67] using periodic boundary conditions and 1 fs time steps. The CHARMM27 force field[68] with CMAP corrections[69,70] and the TIP3P water model[77] for explicit solvent have been applied. The systems were minimized with conjugated gradient method for 1500 steps. The minimization was followed by a 500 ps NVT lipid tail melting at 310 K where everything except the lipid tails are held fixed. The system was equilibrated in a 2 ns constraint free simulation in the NPT ensemble at 1 atm pressure and 310 K. The van der Waals interactions were calculated applying a cutoff distance of 12 Å and switching the potential from 10 Å, and long-range electrostatics were calculated utilizing the particle mesh Ewald (PME) algorithm.[78] Constant pressure of 1 atm was maintained by the Langevin piston method[79] with a piston period of 100 fs and a piston decay of 50 fs. Constant temperature of 310 K is achieved utilizing the Langevin dynamics with a damping constant of 1 ps^{-1} in lipid melting simulation and 5 ps^{-1} in the equilibration phase. The MD simulations were run for 40 ns. The trajectories were analyzed using the program VMD.[76]

Mutagenesis. hNET or hDAT pCDNA inserted into the pCDNA3.1 vector was subjected to mutagenesis by mismatched primer pairs in a polymerase reaction using Phusion (Finnzymes). DNA was purified from overnight XL10 Gold *E. coli* cultures grown in LB media supplemented with 200 ng/mL ampicillin using the PureYield midiprep kit (Promega). Mutant DNA was sequenced across the entire transporter open reading frame using BigDye v3.1 chemistry (Applied Biosystems) analyzed on an ABI 3100 sequencer (Applied Biosystems) to verify that the transporter gene contained the desired mutations and that no unwanted mutations had been introduced.

Cell Culture. HEK293MSR cells (Invitrogen) were cultured in Dulbecco's modified Eagle's medium (BioWhitaker) supplemented with 10% fetal calf serum (Invitrogen), 100 units/mL penicillin, 100 μg/mL streptomycin (BioWhitaker), and 6 μg/mL Geneticin (Invitrogen) at 95% humidity, 5% p(CO_2) at 37 °C. Two days prior to the uptake assay, cells were detached by Versene and trypsin/EDTA treatment and mixed with a preformed complex of transporter DNA and Lipofectamine2000 (Invitrogen). The transfection mix was dispensed into TC-treated white 96-well plates (Nunc) at a cell density of 50−70% confluency and 0.167−0.333 μg DNA/cm^2 and incubated for 50−60 h.

Uptake Inhibition Assay. Adherent transfected cells were washed with PBSCM (137 mM NaCl, 2.7 mM KCl, 4.3 mM Na_2HPO_4, 1.4 mM KH_2PO_4, 0.1 mM $CaCl_2$, and 1 mM $MgCl_2$, pH 7.4) and preincubated for 25 min with a dilution series of the inhibitor. Uptake was initiated by adding a mixture of 50−100 nM [^{3}H]-dopamine (Perkin-Elmer) and the inhibitor at the same concentration as in the preincubation. Radioactive neurotransmitter uptake was allowed to proceed for 10 min at 22 °C and was terminated by washing with PBSCM. Aspirated cells were lysed with Microscint 20 (Packard,) and the accumulated radioactive neurotransmitter quantified on a Packard Topcounter.

Data Analysis. Radioactive counts from accumulated neurotransmitter were fitted from to a sigmoidal dose−response curve in Graphpad Prism 3. The resulting IC_{50} values were transformed to K_i values using the Cheng-Prusoff equation. Statistical comparison of K_i values were conducted using Student's t test.

■ ASSOCIATED CONTENT

Ⓢ Supporting Information

The Supporting Information includes tables of the statistics for homology modeling of hSERT, hDAT, and hNET in Tables S1−S3. Tables S4−S6 report the data for all poses for the induced fit docking calculations. This material is available free of charge via the Internet at http://pubs.acs.org.

■ AUTHOR INFORMATION

Corresponding Author

*Telephone: +45 8942 3953. Fax: +45 8619 6199. E-mail: birgit@chem.au.dk.

Present Address

[§]Structural Bioinformatics and Computational Biochemistry Unit, Department of Biochemistry, University of Oxford, South Parks Road, Oxford OX1 3QU, United Kingdom.

Author Contributions

H.K. did homology modeling, docking calculations, and MD simulations. A.B.C. carried out the SAR experiments with planning by S.S. H.K. and B.S. planned the project and wrote the manuscript with assistance from S.S.

Funding

We gratefully thank The Danish Council for Independent researchlNatural Sciences and the Lundbeck and Carlsberg Foundations for financial support.

Notes

The authors declare no competing financial interest.

■ ACKNOWLEDGMENTS

We thank the Danish Center for Scientific Computing for access to supercomputing facilities.

■ ABBREVIATIONS

hSERT, human serotonin transporter; hDAT, human dopamine transporter; hNET, human norepinephrine transporter; 5-HT, serotonin; DA, dopamine; NE, norepinephrine; LeuT, leucine transporter; IFD, induced fit docking; TM, transmembrane; EL2, extracellular loop 2; dSERT, *Drosophila* SERT; wt, wild type; OCD, obsessive-compulsive disorder; ADHD, attention deficit hyperactivity disorder

REFERENCES

(1) Hahn, M. K., and Blakely, R. D. (2002) Monoamine Transporter Gene Structure and Polymorphisms in Relation to Psychiatric and Other Complex Disorders. *Pharmacogenomics J. 2*, 217−235.

(2) Schloss, P., and Williams, D. C. (1998) The Serotonin Transporter: A Primary Target for Antidepressant Drugs. *J. Psychopharmacol. 12*, 115−121.

(3) Paczkowski, F. A., Sharpe, I. A., Dutertre, S., and Lewis, R. J. (2007) Chi -Conopeptide and Tricyclic Antidepressant Interactions at the Norepinephrine Transporter Define a New Transporter Model. *J. Biol. Chem. 282*, 17837−17844.

(4) Andersen, J., Kristensen, A. S., Bang-Andersen, B., and Strømgaard, K. (2009) Recent Advances in the Understanding of the Interaction of Antidepressant Drugs with Serotonin and Norepinephrine Transporters. *Chem. Commun.*, 3677−3692.

(5) Rudnick, G. (2002) Mechanisms of Biogenic Amine Neurotransmitter Transporters. In *Neurotransmitter Transporters: Structure, Function and Regulation* (Reith, M. E. A., Ed.), 2nd ed., pp 25−52, Humana Press: Totowa, New Jersey.

(6) Dutta, A. K., Zhang, S., Kolhatkar, R., and Reith, M. E. A. (2003) Dopamine Transporter as Target for Drug Development of Cocaine Dependence Medications. *Eur. J. Pharmacol. 479*, 93−106.

(7) Field, J. R., Henry, L. K., and Blakely, R. D. (2010) Transmembrane Domain 6 of the Human Serotonin Transporter Contributes to an Aqueously Accessible Binding Pocket for Serotonin and the Psychostimulant 3,4-Methylenedioxymethamphetamine. *J. Biol. Chem. 285*, 11270−11280.

(8) Yamashita, A., Singh, S. K., Kawate, T., Jin, Y., and Gouaux, E. (2005) Crystal Structure of a Bacterial Homologue of Na^+/Cl^--Dependent Neurotransmitter Transporters. *Nature 437*, 215−223.

(9) Singh, S. K., Piscitelli, C. L., Yamashita, A., and Gouaux, E. (2008) A Competitive Inhibitor Traps LeuT in an Open-to-Out Conformation. *Science 322*, 1655−1661.

(10) Quick, M., Winther, A. L., Shi, L., Nissen, P., Weinstein, H., and Javitch, J. A. (2009) Binding of an Octylglucoside Detergent Molecule in the Second Substrate (S2) Site of LeuT Establishes an Inhibitor-Bound Conformation. *Proc. Natl. Acad. Sci. U.S.A. 106*, 5563−5568.

(11) Kroncke, B. M., Horanyi, P. S., and Columbus, L. (2010) *Structural Origins of Nitroxide Side Chain Dynamics on Membrane Protein α-Helical Sites*, American Chemical Society, Washington, DC.

(12) Zhou, Z., Zhen, J., Karpowich, N. K., Goetz, R. M., Law, C. J., Reith, M. E. A., and Wang, D. (2007) LeuT-Desipramine Structure Reveals how Antidepressants Block Neurotransmitter Reuptake. *Science 317*, 1390−1393.

(13) Singh, S. K., Yamashita, A., and Gouaux, E. (2007) Antidepressant Binding Site in a Bacterial Homologue of Neurotransmitter Transporters. *Nature 448*, 952−956.

(14) Zhou, Z., Zhen, J., Karpowich, N. K., Law, C. J., Reith, M. E. A., and Wang, D. (2009) Antidepressant Specificity of Serotonin Transporter Suggested by Three LeuT-SSRI Structures. *Nat. Struct. Mol. Biol. 16*, 652−658.

(15) Schulze, S., Koster, S., Geldmacher, U., Terwisscha van Scheltinga, A. C., and Kuhlbrandt, W. (2010) Structural Basis of Na^+-Independent and Cooperative substrate/product Antiport in CaiT. *Nature 467*, 233−236.

(16) Shimamura, T., Weyand, S., Beckstein, O., Rutherford, N. G., Hadden, J. M., Sharples, D., Sansom, M. S. P., Iwata, S., Henderson, P. J. F., and Cameron, A. D. (2010) Molecular Basis of Alternating Access Membrane Transport by the Sodium-Hydantoin Transporter Mhp1. *Science 328*, 470−473.

(17) Weyand, S., Shimamura, T., Yajima, S., Suzuki, S., Mirza, O., Krusong, K., Carpenter, E. P., Rutherford, N. G., Hadden, J. M., O'Reilly, J., Ma, P., Saidijam, M., Patching, S. G., Hope, R. J., Norbertczak, H. T., Roach, P. C. J., Iwata, S., Henderson, P. J. F., and Cameron, A. D. (2008) Structure and Molecular Mechanism of a Nucleobase-Cation-Symport-1 Family Transporter. *Science 322*, 709−713.

(18) Shaffer, P. L., Goehring, A., Shankaranarayanan, A., and Gouaux, E. (2009) Structure and Mechanism of a Na+-Independent Amino Acid Transporter. *Science 325*, 1010−1014.

(19) Fang, Y., Jayaram, H., Shane, T., Kolmakova-Partensky, L., Wu, F., Williams, C., Xiong, Y., and Miller, C. (2009) Structure of a Prokaryotic Virtual Proton Pump at 3.2 Å Resolution. *Nature 460*, 1040−1043.

(20) Ressl, S., Terwisscha van Scheltinga, A. C., Vonrhein, C., Ott, V., and Ziegler, C. (2009) *Nature 458*, 47−52.

(21) Faham, S., Watanabe, A., Besserer, G. M., Cascio, D., Specht, A., Hirayama, B. A., Wright, E. M., and Abramson, J. (2008) The Crystal Structure of a Sodium Galactose Transporter Reveals Mechanistic Insights into Na+/Sugar Symport. *Science 321*, 810−814.

(22) Tavoulari, S., Forrest, L. R., and Rudnick, G. (2009) Fluoxetine (Prozac) Binding to Serotonin Transporter is Modulated by Chloride and Conformational Changes. *J. Neurosci. 29*, 9635−9643.

(23) Zhang, Y., and Rudnick, G. (2006) The Cytoplasmic Susbtrate Permeation Pathway of Serotonin Transporter. *J. Biol. Chem. 281*, 36213−36220.

(24) Beuming, T., Shi, L., Javitch, J. A., and Weinstein, H. (2006) A Comprehensive Structure-Based Alignment of Prokaryotic and Eukaryotic Neurotransmitter/Na^+ Symporters (NSS) Aids in the use of the LeuT Structure to Probe NSS Structure and Function. *Mol. Pharmacol. 70*, 1630−1642.

(25) Jørgensen, A. M., Tagmose, L., Jørgensen, A. M. M., Bøgesø, K. P., and Peters, G. H. (2007) Molecular Dynamics Simulations of Na^+/Cl^--Dependent Neurotransmitter Transporters in a Membrane-Aqueous System. *ChemMedChem 2*, 827−840.

(26) Celik, L., Sinning, S., Severinsen, K., Hansen, C., Møller, M., Bols, M., Wiborg, O., and Schiøtt, B. (2008) Binding of Serotonin to the Human Serotonin Transporter. Molecular Modeling and Experimental Validation. *J. Am. Chem. Soc. 130*, 3853−3865.

(27) Kaufmann, K. W., Dawson, E. S., Henry, L. K., Field, J. R., Blakely, R. D., and Meiler, J. (2009) Structural Determinants of Species-Selective Substrate Recognition in Human and *Drosophila* Serotonin Transporters Revealed through Computational Docking Studies. *Proteins: Struct., Funct., Bioinf. 74*, 630−642.

(28) Sinning, S., Musgaard, M., Jensen, M., Severinsen, K., Celik, L., Koldsø, H., Meyer, T., Bols, M., Jensen, H. H., Schiøtt, B., and Wiborg, O. (2010) Binding and Orientation of Tricyclic Antidepressants within the Central Substrate Site of the Human Serotonin Transporter. *J. Biol. Chem. 285*, 8363−8374.

(29) Koldsø, H., Severinsen, K., Tran, T. T., Celik, L., Jensen, H. H., Wiborg, O., Schiøtt, B., and Sinning, S. (2010) The Two Enantiomers of Citalopram Bind to the Human Serotonin Transporter in Reversed Orientations. *J. Am. Chem. Soc. 132*, 1311−1322.

(30) Indarte, M., Madura, J., and Surratt, C. (2008) Dopamine Transporter Comparative Molecular Modeling and Binding Site Prediction using the $LeuT_{Aa}$ Leucine Transporter as a Template. *Proteins: Struct., Funct., Bioinf. 70*, 1033−1046.

(31) Beuming, T., Kniazeff, J., Bergmann, M. L., Shi, L., Gracia, L., Raniszewska, K., Newman, A. H., Javitch, J. A., Weinstein, H., Gether, U., and Loland, C. J. (2008) The Binding Sites for Cocaine and Dopamine in the Dopamine Transporter Overlap. *Nat. Neurosci. 11*, 780−789.

(32) Ravna, A., Sylte, I., and Dahl, S. (2009) Structure and Localisation of Drug Binding Sites on Neurotransmitter Transporters. *J. Mol. Model. 15*, 1155−1164.

(33) Schlessinger, A., Geier, E., Fan, H., Irwin, J. J., Shoichet, B. K., Giacomini, K. M., and Sali, A. (2011) Structure-Based Discovery of Prescription Drugs that Interact with the Norepinephrine Transporter, NET. *Proc. Natl. Acad. Sci. U.S.A. 108*, 15810−15815.

(34) Gaffaney, J. D., and Vaughan, R. A. (2004) Uptake Inhibitors but Not Substrates Induce Protease Resistance in Extracellular Loop Two of the Dopamine Transporter. *Mol. Pharmacol. 65*, 692−701.

(35) Chen, J., Liu-Chen, S., and Rudnick, G. (1997) External Cysteine Residues in the Serotonin Transporter†. *Biochemistry. 36*, 1479−1486.

(36) Chen, R., Wei, H., Hill, E., Chen, L., Jiang, L., Han, D., and Gu, H. (2007) Direct Evidence that Two Cysteines in the Dopamine Transporter Form a Disulfide Bond. *Mol. Cell. Biochem. 298*, 41−48.
(37) Tate, C. G., and Blakely, R. D. (1994) The Effect of N-Linked Glycosylation on Activity of the Na^+- and Cl^--Dependent Serotonin Transporter Expressed using Recombinant Baculovirus in Insect Cells. *J. Biol. Chem. 269*, 26303−26310.
(38) Melikian, H. E., Ramamoorthy, S., Tate, C. G., and Blakely, R. D. (1996) Inability to N-Glycosylate the Human Norepinephrine Transporter Reduces Protein Stability, Surface Trafficking, and Transport Activity but Not Ligand Recognition. *Mol. Pharmacol. 50*, 266−276.
(39) Parnas, M. L., and Vaughan, R. A. (2008) Molecular Structure and Composition of Dopamine Transporters. In *Dopamine Transporters: Chemistry, Biology, and Pharmacology* (Trudell, M. L., an Izenwasser, S., Ed), pp 73−95, John Wiley & Sons, Inc.: Hoboken, New Jersey
(40) Rasmussen, T. N., Plenge, P., Bay, T., Egebjerg, J., and Gether, U. (2009) A Single Nucleotide Polymorphism in the Human Serotonin Transporter Introduces a New Site for N-Linked Glycosylation. *Neuropharmacology 57*, 287−294.
(41) Eswar, N., Webb, B., Marti-Renom, M. A., Madhusudhan, M. S., Eramian, D., Shen, M., Pieper, U., and Sali, A. (2007) Comparative Protein Structure Modeling using MODELLER. *Curr. Protoc. Prot. Sci. 2*, 1−2.9.
(42) Sali, A., and Blundell, T. L. (1993) Comparative Protein Modelling by Satisfaction of Spatial Restraints. *J. Mol. Biol. 234*, 779−815.
(43) Jørgensen, A. M., Tagmose, L., Jørgensen, A. M. M., Topiol, S., Sabio, M., Gundertofte, K., Bøgesø, K. P., and Peters, G. H. (2007) Homology Modeling of the Serotonin Transporter: Insights into the Primary Escitalopram-Binding Site. *ChemMedChem 2*, 815−826.
(44) Sherman, W., Day, T., Jacobson, M. P., Friesner, R. A., and Farid, R. (2006) Novel Procedure for Modeling Ligand/Receptor Induced Fit Effects. *J. Med. Chem. 49*, 534−553.
(45) Rudnick, G. (2006) Serotonin Transporters - Structure and Function. *J. Membr. Biol. 213*, 101−110.
(46) Nelson, P. J., and Rudnick, G. (1979) Coupling between Platelet 5-Hydroxytrypthamine and Potassium Transport. *J. Biol. Chem. 254*, 10084−10089.
(47) Gu, H., Wall, S. C., and Rudnick, G. (1994) Stable Expression of Biogenic Amine Transporters Reveals Differences in Inhibitor Sensitivity, Kinetics, and Ion Dependence. *J. Biol. Chem. 269*, 7124−7130.
(48) Gu, H. H., Wall, S., and Rudnick, G. (1996) Ion Coupling Stoichiometry for the Norepinephrine Transporter in Membrane Vesicles from Stably Transfected Cells. *J. Biol. Chem. 271*, 6911−6916.
(49) Forrest, L. R., Tavoulari, S., Zhang, Y. W., Rudnick, G., and Honig, B. (2007) Identification of a Chloride Ion Binding Site in Na^+/Cl^--Dependent Transporters. *Proc. Natl. Acad. Sci. U.S.A. 104*, 12761−12766.
(50) Zomot, E., Bendahan, A., Quick, M., Zhao, Y., Javitch, J., and Kanner, B. (2007) Mechanism of Chloride Interaction with Neurotransmitter:Sodium Symporters. *Nature 449*, 726−730.
(51) Topiol, S. (1987) The Deletion Model for the Origin of Receptors. *Trends Biochem. Sci. 12*, 419−421.
(52) Zhao, C., and Noskov, S. Y. (2011) The Role of Local Hydration and Hydrogen-Bonding Dynamics in Ion and Solute Release from Ion-Coupled Secondary Transporters. *Biochemistry 50*, 1848−1856.
(53) Koldsø, H., Noer, P., Autzen, H. E., Grouleff, J., Sinning, S., and Schiøtt, B. (2011) Unbiased Simulations Reveal the Inward-Facing Conformation of the Human Serotonin Transporter and Na^+ Ion Release. *PLoS Comput. Biol. 7* (10), e1002246.
(54) Yu, H., Noskov, S. Y., and Roux, B. (2010) Two Mechanisms of Ion Selectivity in Protein Binding Sites. *Proc. Natl. Acad. Sci. U.S.A. 107*, 20329−20334.
(55) Noskov, S. Y., and Roux, B. (2008) Control of Ion Selectivity in LeuT: Two Na+ Binding Sites with Two Different Mechanisms. *J. Mol. Biol. 377*, 804−818.
(56) Huang, X., and Zhan, C. (2007) How Dopamine Transporter Interacts with Dopamine: Insights from Molecular Modeling and Simulation. *Biophys. J. 93*, 3627−3639.
(57) Henry, L. K., Field, J. R., Adkins, E. M., Parnas, M. L., Vaughan, R. A., Zou, M. F., Newman, A. H., and Blakely, R. D. (2006) Tyr95 and Ile172 in Transmembrane Segments 1 and 3 of Human Serotonin Transporters Interact to Establish High-Affinity Recognition of Antidepressants. *J. Biol. Chem. 281*, 2012−2023.
(58) Barker, E. L., Perlman, M. A., Adkins, E. M., Houlihan, W. J., Pristupa, Z. B., Niznik, H. B., and Blakely, R. D. (1998) High Affinity Recognition of Serotonin Transporter Antagonists Defined by Species-Scanning Mutagenesis. *J. Biol. Chem. 273*, 19459−19468.
(59) Chen, N., and Reith, M. E. A. (2002) Structure-Function Relationship for Biogenic Amine Neurotransmitter Transporters. In *Neurotransmitter Transporters: Structure, Function and Regulation* (Reith, M. E. A., Ed.), 2nd ed., pp 53−109, Humana Press: Totowa, New Jersey.
(60) Eshleman, A. J., Carmolli, M., Cumbay, M., Martens, C. R., Neve, K. A., and Janowsky, A. (1999) Characteristics of Drug Interactions with Recombinant Biogenic Amine Transporters Expressed in the Same Cell Type. *J. Pharmacol. Exp. Ther. 289*, 877−885.
(61) Larsen, M. B., Sonders, M. S., Mortensen, O. V., Larson, G. A., Zahniser, N. R., and Amara, S. G. (2011) Dopamine Transport by the Serotonin Transporter: A Mechanistically Distinct Mode of Substrate Translocation. *J. Neurosci. 31*, 6605−6615.
(62) Andersen, J., Taboureau, O., Hansen, K. B., Olsen, L., Egebjerg, J., Strømgaard, K., and Kristensen, A. S. (2009) Location of the Antidepressant Binding Site in the Serotonin Transporter: Importance of Ser-438 in the Recognition of Citalopram and Tricyclic Antidepressants. *J. Biol. Chem. 284*, 10276−10284.
(63) Manepalli, S., Surratt, C. K., Madura, J., and Nolan, T. L. (2012) Monoamine Transporter Structure, Function, Dynamics and Drug Discovery: A Computational Perspective. *AAPS J. 14*, 820−831.
(64) Thomsen, R., and Christensen, M. H. (2006) MolDock: A New Technique for High-Accuracy Molecular Docking. *J. Med. Chem. 49*, 3315−3321.
(65) Laskowski, R. A., MacArthur, M. W., Moss, D. S., and Thornton, J. M. (1993) PROCHECK: A Program to Check the Stereochemical Quality of Protein Structures. *J. Appl. Crystallogr. 26*, 283−291.
(66) Kalé, L., Skeel, R., Bhandarkar, M., Brunner, R., Gursoy, A., Krawetz, N., Phillips, J., Shinozaki, A., Varadarajan, K., and Schulten, K. (1999) NAMD2: Greater Scalability for Parallel Molecular Dynamics. *J. Comput. Phys. 151*, 283−312.
(67) Phillips, J. C., Braun, R., Wang, W., Gumbart, J., Tajkhorshid, E., Villa, E., Chipot, C., Skeel, R. D., Kalé, L., and Schulten, K. (2005) Scalable Molecular Dynamics with NAMD. *J. Comput. Chem. 26*, 1781−1802.
(68) MacKerell, A. D. J., Bashford, D., Bellott, M., Dunbrack, R. L., Jr., Evanseck, J. D., Field, M. J., Fischer, S., Gao, J., Guo, H., Ha, S., Joseph-McCarthy, D., Kuchnir, L., Kuczera, K., Lau, F. T. K., Mattos, C., Michnick, S., Ngo, T., Nguyen, D. T., Prodhorn, B., Reiher, W. E., III, Roux, B., Schlenkrich, M., Smith, J. C., Stote, R., Straub, J., Watanabe, M., Wiórkiewicz-Kuczera, J., Yin, D., and Karplus, M. (1998) All-Atom Empirical Potential for Molecular Modeling and Dynamics Studies of Proteins. *J. Phys. Chem. B 102*, 3586−3616.
(69) MacKerell, A. D. J., Feig, M., and Brooks, C. L., III. (2004) Extending the Treatment of Backbone Energetics in Protein Force Fields: Limitations of Gas-Phase Quantum Mechanics in Reproducing Protein Conformational Distributions in Molecular Dynamics Simulations. *J. Comput. Chem. 25*, 1400−1415.
(70) MacKerell, A. D. J., Feig, M., and Brooks, C. L., III. (2004) Improved Treatment of the Protein Backbone in Empirical Force Fields. *J. Am. Chem. Soc. 126*, 698−699.
(71) Schrödinger LLC (2008) Schrödinger Suite 2008, Maestro Version 8.5, MacroModel Version 9.6, Glide Version 5.0, Prime Version 2.0, New York, NY, 2008.

(72) Kaminski, G. A., Friesner, R. A., Tirado-Rives, J., and Jorgensen, W. L. (2001) Evaluation and Reparametrization of the OPLS-AA Force Field for Proteins Via Comparison with Accurate Quantum Chemical Calculations on Peptides. *J. Phys. Chem. B 105*, 6474−6487.
(73) Friesner, R. A., Banks, J. L., Murphy, R. B., Halgren, T. A., Klicic, J. J., Mainz, D. T., Repasky, M. P., Knoll, E. H., Shelley, M., Perry, J. K., Shaw, D. E., Francis, P., and Shenkin, P. S. (2004) Glide: A New Approach for Rapid, Accurate Docking and Scoring. 1. Method and Assessment of Docking Accuracy. *J. Med. Chem. 47*, 1739−1749.
(74) Friesner, R. A., Murphy, R. B., Repasky, M. P., Frye, L. L., Greenwood, J. R., Halgren, T. A., Sanschagrin, P. C., and Mainz, D. T. (2006) Extra Precision Glide: Docking and Scoring Incorporating a Model of Hydrophobic Enclosure for Protein-Ligand Complexes. *J. Med. Chem. 49*, 6177−6196.
(75) Li, H., Robertson, A. D., and Jensen, J. H. (2005) Very Fast Empirical Prediction and Rationalization of Protein pK_a Values. *Proteins: Struct., Funct., Bioinf. 61*, 704−721.
(76) Humphrey, W., Dalke, A., and Schulten, K. (1996) VMD: Visual Molecular Dynamics. *J. Mol. Graphics 14*, 33−38.
(77) Jorgensen, W. L., Chandrasekhar, J., Madura, J. D., Impey, R. W., and Klein, M. L. (1983) Comparison of Simple Potential Functions for Simulating Liquid Water. *J. Chem. Phys. 79*, 926−935.
(78) Darden, T., York, D., and Pedersen, L. (1993) Particle Mesh Ewald: An *N* *log(*N*) Method for Ewald Sums in Large Systems. *J. Chem. Phys. 98*, 10089−10092.
(79) Feller, S. E., Zhang, Y., Pastor, R. W., and Brooks, B. R. (1995) Constant Pressure Molecular Dynamics Simulation: The Langevin Piston Method. *J. Chem. Phys. 103*, 4613−4621.